# CERAMIC SENSORS III


Edited by

H. U. Anderson
M. Liu
N. Yamazoe

Published by:

The Electrochemical Society, Inc.
10 South Main Street
Pennington, New Jersey 08534-2896, USA

Telephone (609) 737-1902
Fax (609) 737-2743
e-mail: ecs@electrochem.org
Web site: http://www.electrochem.org

ISBN 1-56677-127-7

Printed in the United States of America

Published by:

The Electrochemical Society, Inc.
10 South Main Street
Pennington, New Jersey 08534-2896, USA

Telephone (609) 737-1902
Fax (609) 737-2743
e-mail: ecs@electrochem.org
Web site: http://www.electrochem.org

ISBN 1-56677-127-7

Printed in the United States of America

# Preface

Ceramic sensors play an increasingly important role in process control and automation and in environmental monitoring and protection. This proceedings volume contains 21 of the 23 papers presented at the Symposium on Ceramic Sensors III, held during the 190th Meeting of The Electrochemical Society in San Antonio, Texas, October 6-11, 1996. The papers cover various aspects of ceramic sensors based on physical, optical, and electrochemical principles. Materials used for sensors include insulators, semiconductors, ionic conductors, mixed ionic-electronic conductors, and zeolites in the form of particles, thin films, membranes, coatings, and junctions. Some of the papers focus on synthesis and processing of sensor materials, others on design, fabrication, and evaluation of sensing devices, and still others on exploration, characterization, and modeling of transport properties, catalytic activities, electrode kinetics, and stability of materials suitable for sensor applications. In particular, recent developments in sensors for ammonia ($NH_3$), carbon monoxide (CO), carbon dioxide ($CO_2$), nitrogen oxides ($NO_x$), humidity ($H_2O$), hydrogen ($H_2$), hydrocarbons, and human activities are discussed.

# FACTS ABOUT THE ELECTROCHEMICAL SOCIETY, INC.

The Electrochemical Society, Inc., is an international, nonprofit, scientific, educational organization founded for the advancement of the theory and practice of electrochemistry, electrothermics, electronics, and allied subjects. The Society was founded in Philadelphia in 1902 and incorporated in 1930. There are currently over 7000 scientists and engineers from more than 60 countries who hold individual membership; the Society is also supported by more than 100 corporations through Patron and Sustaining Memberships.

The Technical activities of the Society are carried on by Divisions and Groups. Local Sections of the Society have been organized in a number of cities and regions.

Major international meetings of the Society are held in the Spring and Fall of each year. At these meetings, the Divisions and Groups hold general sessions and sponsor symposia on specialized subjects.

The Society has an active publications program which includes the following:

**Journal of The Electrochemical Society** - The **Journal** is a monthly publication containing technical papers covering basic research and technology of interest in the areas of concern to the Society. Papers submitted for publication are subjected to careful evaluation and review by authorities in the field before acceptance, and high standards are maintained for the technical content of the **Journal**.

**Interface** - Interface is a quarterly publication containing news, reviews, advertisements, and articles on technical matters of interest to Society Members in a lively, casual format. Also featured in each issue are special pages dedicated to serving the interests of the Society and allowing better communication between Divisions, Groups, and Local Sections.

**Meeting Abstracts** *(formerly Extended Abstracts)* - Meeting Abstracts of the technical papers presented at the Spring and Fall Meetings of the Society are published in serialized softbound volumes.

**Proceedings Series** - Papers presented in symposia at Society and Topical Meetings are published from time to time as serialized Proceedings Volumes. These provide up-to-date views of specialized topics and frequently offer comprehensive treatment of rapidly developing areas.

**Monograph Volumes** - The Society has, for a number of years, sponsored the publication of hardbound Monograph Volumes, which provide authoritative accounts of specific topics in electrochemistry, solid state science, and related disciplines.

For more information on these and other Society activities, visit the ECS Home Page at the following address on the World Wide Web:

**http://www.electrochem.org.**

## Table of Contents

# MIEC SOLID OXIDE MEMBRANES WITH POROUS ELECTRODES

B. Abeles
Department of Chemistry, University of Houston,
Houston, TX 77204-5641

## ABSTRACT

Numerical solution of the nonlinear diffusion-reaction equations for MIEC membrane with charge carrier density that varies only weakly with gas pressure show that the enhancement in oxygen flux, due to porous electrodes, is essentially independent of the magnitude of the pressure gradient. Enhancements in oxygen flux of two orders in magnitude are theoretically achievable with large surface area electrodes.

## INTRODUCTION

Electrocatalytic fuel cells and membranes consist in general of a porous cathode and anode separated by a dense layer, as illustrated in Fig.1. The purpose of the porous layers is to increase the surface area for exchange of oxygen to enhance the oxygen flux, while the dense layer blocks the passage of oxygen molecules. In the case of a fuel cell this dense layer is an ionic conductor allowing the passage of ions but blocking that of electrons, while in the case of a membrane the dense layer is a mixed ionic electronic conductor (MIEC) which allows the passage of electrons as well as ions.

In this paper we focus on solid oxide MIEC membranes, however the results can be readily extended to fuel cells. In the application of membranes as chemical reactors or for separation of gases, we are interested in the upper limit of oxygen flux that can be achieved for a given pressure drop across the membrane. The oxygen flux in the dense membrane can be increased by reducing the thickness of the membrane until it is less than $L_d$ where $L_d$ is the ratio of the ambipolar ion-electron hole pair diffusion coefficient to the surface chemical reaction rate coefficient (1,2). The length scale $L_d$ determines the transition from bulk diffusion limited to surface chemical reaction rate limited transport in the dense membrane. Any further increase in the ion current can be achieved only by coating the dense layer with porous layers so as to increase the effective area for chemical reaction. In the following we discuss how the enhancement in the oxygen flux depends on the length scales given by $L_d$, the thickness of the dense layer $\ell$, the thickness of the porous layers L and the width of the chemical reaction zones $L_p$ at the dense-porous layer interfaces.

## MODEL

The chemical reaction at the gas-solid interfaces is given by

$$\frac{1}{2}O_2 \Leftrightarrow O^{2-} + 2h \qquad [1]$$

The diffusion of oxygen molecules in the pores and of oxygen ion-electron hole pairs in the porous solid are described by the molecular current $I_g$ and ion current $I_i$ (3-5):

$$I_g = -\frac{\phi}{\tau_g}\frac{c_g D_g}{RT}\frac{d\mu_g}{dx} \qquad [2]$$

$$I_i = -\frac{1-\phi}{\tau_s}\frac{c_i D_a}{RT}\frac{d\mu}{dx} \qquad [3]$$

$$\mu_g = RT\ln(p/p_0) \qquad [4]$$

$$D_a = D_i\sigma_e/(\sigma_e+\sigma_i) \qquad [5]$$

where $\mu_g$ and $\mu$ are the chemical potentials of the gas molecules and of the oxygen ion-electron hole pairs, $D_g$ and $D_i$ are the diffusion coefficients of the gas in the pores and of the oxygen ions in the solid, $D_a$ is the ambipolar diffusion coefficient of the oxygen ion-electron hole pairs, $\sigma_e$ and $\sigma_i$ are the electronic and ionic conductivities, $c_g$ and $c_i$ are the concentrations of the gas molecules in the pores and of the ions in the solid, $\phi$ is the porosity and $\tau_g$ the tortuosity of the pores, $\tau_s$ the tortuosity of the solid, p is the gas pressure and the subscript 0 indicates quantities at 1 atm. pressure. Equation (3) applies in the dense layer with $\tau_s=1$ and $\phi=0$. In general the transport coefficients can assume different values in each one of the three layers.

The chemical reaction at the pore wall-gas interfaces in the porous layer on the high pressure side of the membrane results in an a decrease in $I_g$ and a corresponding increase in $I_i$ with increasing x, while in the porous layer on the low pressure side of the membrane $I_g$ increases and $I_i$ decreases with x. This is quantitatively described by the equations:

$$\frac{dI_g}{dx} = -\frac{1}{2}Si, \qquad [6]$$

$$\frac{dI_i}{dx} = Si, \qquad [7]$$

where S is the pore surface area per unit volume and i is the surface exchange current.

We next need to specify the dependence of i on the drop in chemical potential across the gas-solid interface. Lee et al (6) showed that the pressure dependence of the oxygen permeation flux $J_{O2}^{(s)}$ in thin dense $SrCo_{0.8}Fe_{0.2}O_{3-d}$ membranes in the surface exchange limited regime ($\ell \ll L_d$) follows a square root behavior given by:

$$J_{O2}^{(s)} = (c_i k_{i0} / 4)(\sqrt{p_1 / p_0} - \sqrt{p_2 / p_0}) \qquad [8]$$

where $p_1$ and $p_2$ are the oxygen pressures on the high and low pressure sides of the membrane. The square root behavior is consistent with a surface exchange current given by:

$$i = c_i k_{i0} [\exp(\mu_g / 2RT) - \exp(\mu / RT)] \qquad [9]$$

where $k_{i0}$ is the surface exchange coefficient at 1 atm pressure and $\mu_g$ and $\mu$ are evaluated at the interface.

The solution to Eqs.(2)-(7) must fit the boundary conditions:

$$-\frac{1-\phi}{\tau_s}\frac{c_i D_a}{RT}\frac{d\mu}{dx} = \pm(1-\phi)i \qquad \text{at } x = \mp\frac{1}{2}(L+\ell) \qquad [10]$$

$$\mu_g = \mu_{g1} \qquad \text{at } x = -\frac{1}{2}(L+\ell) \qquad [11]$$

$$\mu_g = \mu_{g2} \qquad \text{at } x = \frac{1}{2}(L+\ell) \qquad [12]$$

$$I_g = \pm\frac{1}{2}\phi i \qquad \text{at } \mp\frac{1}{2}\ell \qquad [13]$$

$$I_i = 2J_{O2} = -\frac{c_i D_a}{RT\ell}[\mu(\ell/2) - \mu(-\ell/2)] \qquad -\ell/2<x<\ell/2 \qquad [14]$$

$$J_{O2} = I_g \pm \frac{1}{2}\phi i \quad \text{at} \quad x = \mp\frac{1}{2}(L+\ell) \qquad [15]$$

Equation (10) equates the ion current to the chemical reaction current at the outer porous layer-gas interfaces, Eqs.(11) and (12) fix the gas pressures at the outer porous layer-gas interfaces and Eq.(13) expresses the condition that the dense layer at the center of the membrane blocks the molecular gas flow. Equation (14) relates the total oxygen flux $J_{O2}$ passing through the membrane to the ion current $I_i$ diffusing through the dense layer. Equation (15) relates $J_{O2}$ to $I_g$ at the outer MIEC-gas interface and x=o is taken at the center of the dense layer.

The flux enhancement $\eta$ is defined by:

$$\eta = I_{O2} / I_{O2}^{(s)} \qquad [16]$$

where $J_{O2}^{(s)}$ is the oxygen flux in the absence of the porous layers given by(6):

where $J_{O2}^{(s)}$ is the oxygen flux in the absence of the porous layers given by(6):

$$2J_{O2}^{(s)} / c_i k_{i0} = \frac{L_{d0}}{l} \ln \frac{\sqrt{p_1 / p_0} - 2J_{O2}^{(s)} / c_i k_{i0}}{\sqrt{p_2 / p_0} + 2J_{O2}^{(s)} / c_i k_{i0}} \qquad [17]$$

and $L_{d0}=D_a/k_{i0}$. Note that in the limit $\ell \rightarrow 0$ Eq.(17) reduces to Eq.(8)

In the limit of small pressure drop across the membrane, i.e.$l(\mu_g/2 -\mu)l/RT<<1$, Eq.(9) reduces to the small pressure gradient limit (2-5), $i = c_i k_i (\mu_g / 2 - \mu)$, where $k_i = \sqrt{p / p_0} k_{i0}$, $L_d = \sqrt{p_0 / p} L_{d0}$ and the linearized diffusion-reaction equation can now be solved analytically. For the case where the pressure drop across the porous layers is negligible compared to the pressure drop across the dense layer, the oxygen flux enhancement for an asymmetric membrane with a finite dense layer thickness can be expressed by a simple analytical expression (5):

$$\frac{1}{\eta(\ell)} = \{\frac{k_i c_i}{2}[\frac{1}{(k_i c_i \eta(0))_1} + \frac{1}{(k_i c_i \eta(0))_2}] + \frac{\ell}{2L_d}\} / (1 + \frac{\ell}{2L_d}) \qquad [18]$$

where the subscripts 1 and 2 indicate the two porous layers, the coefficients without numerical subscript refer to the dense layer and $\eta(0)$ is the enhancement of the symmetric membrane with $\ell=0$ (3):

$$\eta(0) = \sqrt{\frac{L_d(1-\phi)S}{\tau_s}} \frac{a \exp(L / L_p) - 1}{a \exp(L / L_p) + 1} + \phi, \qquad [19]$$

$$a = (1 + \sqrt{\frac{\tau_s(1-\phi)}{SL_d}}) / (1 - \sqrt{\frac{\tau_s(1-\phi)}{SL_d}}) \qquad [20]$$

and $L_p$ is the width of the chemically active zones at the dense layer-porous layer interfaces:

$$L_p = \sqrt{L_d(1-\phi) / \tau_s S} \qquad [21]$$

## DISCUSSION AND RESULTS

We model the porous layers by a cubic array of consolidated spherical grains of radius r, with unit cell of length 2(r-δ). The ratio δ/r characterizes the degree of consolidation of the grains. Assuming δ/r=0.1, which corresponds to a well consolidated grain structure, the simple cubic model yields $S=2.2(1-\phi)/r$, $1-\phi=0.69$, $\tau_S=1.16$ and $\tau_g=2$

(3). We use the relation $D_g = \frac{1}{3} v_{th} \lambda$, where $v_{th}$ is the thermal velocity of the molecules, $\lambda$ is the molecular mean free path in the pores determined from $\lambda^{-1} = \lambda_{th}^{-1} + \lambda_p^{-1}$, $\lambda_{th}$ is the thermal mean free path of the molecules and $\lambda_p$ is an average pore size. We take $\lambda_p$ to be the diameter of a sphere whose volume is equal to that of the pore space in the unit cell of the cubic array. For the case of $\delta/r=0.1$ it follows (3) that $\lambda_p=1.5r$. At 800 $^oC$ we have $v_{th}=8.1 \times 10^4$cm/sec, $c_g = 7.3 \times 10^{18} p/p_o$ cm$^{-3}$ and $\lambda_{th}=0.24 p_o/p$ μm.

Equations(2)-(16) were solved numerically (4) by the shooting method. We neglected in Eq.(3) the dependence of $c_i$ and $D_a$ on chemical potential. This assumption is justified in MIEC materials such as $SrCo_{0.8}Fe_{0.2}O_{3-\delta}$ (7). We used representative values (2) for the transport parameters of MIEC materials at 800C: $K_{i0} = 5 \times 10^{-5}$ cm/sec, $D_a = 5 \times 10^{-7}$cm$^2$/sec and $c_i = 0.083$ mol/ cm$^3$.

Figure 2 shows the dependence of $J_{O2}$ and $\eta(\ell)$ on outlet pressure $p_2$ with $p_1$=1atm amd L=4mμ. for a symmetric membrane with $\ell=0$ and for a surface area $S=10^6$cm$^{-1}$(4). After first rising rapidly with increasing pressure gradient, $J_{O2}$ reaches saturation at the low values of $p_2$. The scaling behavior of $J_{O2}$with $J_{O2}^{(s)}$ is demonstrated by the fact that $\eta$ is essentially constant over the whole range of $p_2$ and is close to the value of the enhancement in the small pressure gradient limit, shown by the open circle. We expect this scaling behavior to hold as well for membranes with other functional dependencies of the surface exchange current then that given by Eq.(9) as long as the charge carrier concentration does not vary too rapidly with pressure.

As is demonstrated in Fig.2 the enhancement in the low pressure gradient limit approximates well the enhancement for the case of large pressure gradient and thus is useful as a guide for designing membranes. Figure 3 shows the enhancement $\eta(0)$ calculated from Eq.(19). for a symmetric membrane for different values of the surface area S with $L_d$=0.01cm. The enhancement rises linearly with $L/L_p$ and then saturates for $L>3L_p$. As L is further increased the pressure drop on the low pressure electrode becomes significant resulting in a decrease in $\eta(0)$ (3). Figure 4 shows the dependence of $\eta(\ell)/\eta(0)$ on the thickness of the dense layer $\ell$ calculated from Eq.(18). To achieve full enhancement requires $\ell << L_d / \eta$ Values for the different length scales calculated from Eqs.(19) and (21) are displayed in Table I. Enhancements of two orders of magnitude in the oxygen flux are predicted for membrane with porous electrodes having surface area of $10^6$cm$^{-1}$ (~20 m$^2$/gm) a typical value for a highly dispersed catalyst.

Table I: Length scales and enhancement for MIEC membrane with $L_d$=0.01cm, L=∞, $\ell=0$

| r (μm) | S (cm$^{-1}$) | $L_p$ (μm) | $L_d/\eta$ (μm) | $\eta(\ell)$ |
|---|---|---|---|---|
| 0.015 | $10^6$ | 0.77 | 1.3 | 77 |
| 1.5 | $10^4$ | 7.7 | 13 | 7.7 |

REFERENCES

1.1. B.C.H. Steele, Solid State Ionics, **75**, 157 (1995).
2. H. J. M. Bouwmeester et al,Solid State Ionics, **72**, (1994) 185
3. H. Deng, M.Zhou and B. Abeles, Solid State Ionics, **74**, (1994) 75; **80**, (1995) 213
4. M.Zhou H, Deng and B. Abeles, Solid State Ionics, in print.
5. T.H. Lee, Y.L. Yang, A.J. Jacobson and B. Abeles, to be published
6. T.H. Lee, Y.L. Yang, A.J. Jacobson and B. Abeles, Ceramic Sensors, Electrochemical Society, San Antonio 1996, and forthcoming publication.
7.L.M.Liu, T.H.Lee,.L.Qui, Y.L.Yang and A.J.Jacobson, Mat Res Bull. **31,** (1996) 29


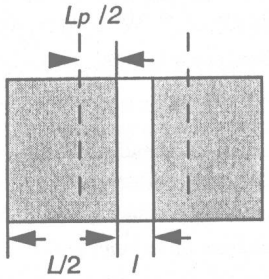


Fig.1. Schematic of MIEC membrane L/2 and $\ell$ are the thicnesses of the porous and dense layers, $L_p$ is the width of the chemically active zone.

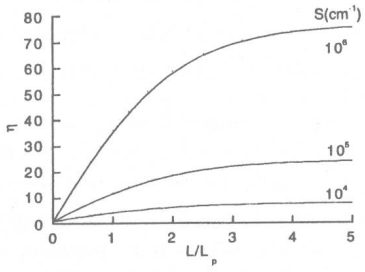


Fig.3. Enhancement $\eta(0)$ as a function of normalized porous layer thickness $L/L_p$ and surface area S, with $L_d = 0.01$cm, calculated from Eq.(19).

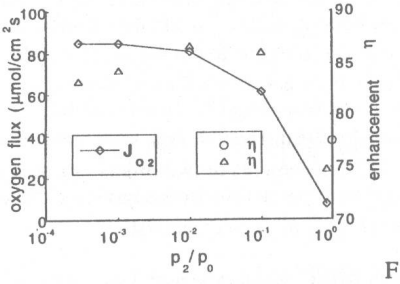


Fig.2. Flux $J_{O2}$ and enhancement $\eta(0)$ as a function of outlet pressure $p_2$ with $p_1$=1atm and L=4μm, calculated from Eqs.(2)-(17); $\eta(0)$ given by open circle (o) calculated from Eq.(19).

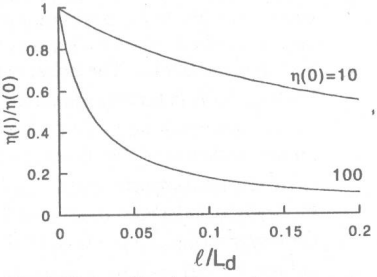


Fig.4. Normalized flux enhancement $\eta(\ell)/\eta(0)$ as a function of normalized dense layer thickness $\ell/L_d$ calculated from Eq.(18)

# IMPROVEMENT ON Sr- AND Mg- DOPED $LaGaO_3$ PEROVSKITE SOLID ELECTROLYTE

Keqin Huang, Man Feng and John B. Goodenough
Center for Materials Science and Engineering ETC 9.102
University of Texas at Austin, Austin, TX78712

A second phase, $LaSrGaO_4$, has been identified in the doped $LaGaO_3$ materials. The elimination of this second phase, which enhances the electrical conductivity, has been achieved by nonstoichiometric doping. Conductivity measurements vs atmosphere and time indicate that this material is a pure oxide-ion conductor with excellent stability. Preliminary single fuel-cell tests gave a high open-circuit voltage and maximum power-density output at 800 °C. These results indicate that doped $LaGaO_3$ is a potential electrolyte material for use in thick-film solid oxide fuel cells.

## INTRODUCTION

The perovskite $LaGaO_3$ doped with Sr and Mg has recently been shown to be a superior oxide-ion conductor at intermediate temperatures (1-4). It has a transport number $t_o \equiv \sigma_o/\sigma \approx 1$ with an oxide-ion conductivity $\sigma_o > 0.1$ S/cm at 800 °C over a broad range of atmosphere from pure oxygen to moistened hydrogen ( $H_2$+3% $H_2O$). These properties make it a strong candidate to replace the commercially available yttria-doped zirconia in solid oxide fuel cells (SOFCs).

Although this doped perovskite system shows promise, discrepancies in published data result from incomplete characterization of the materials studied. For example, Ishihara (1) showed a Sr solubility limit for $La_{1-x}Sr_xGa_{1-y}Mg_yO_{3-\delta}$, $\delta$=0.5(x+y), of x = 0.1 and a Mg solubility limit of y = 0.2 in the cation stoichiometric perovskites whereas Huang and Petric (4) have presented a broader single-phase region with an orthorhombic structure for the Ishihara composition. Unfortunately no x-ray diffraction (XRD) patterns were given by Huang and Petric to support their assertions, and small peaks contributed from a second phase could have been incorrectly interpreted.

In this paper we report the existence of a second phase, identified as $LaSrGaO_4$, in the nominally cation-stoichiometric phase $La_{0.9}Sr_{0.1}Ga_{0.8}Mg_{0.2}O_{2.85}$, which we refer to hereinafter as LSGM. We also present the enhanced oxide-ion conductivity $\sigma_o$ of a cation-nonstoichiometric phase that has been characterized by scanning electron microscopy (SEM) as well as XRD and impedance spectroscopy.

## EXPERIMENTAL PROCEDURE

Preparation of Electrolytes

The new composition LSGM-B was made by solid-state reaction, the same as $La_{0.9}Sr_{0.1}Ga_{0.8}Mg_{0.2}O_{2.85}$ (LSGM) described in ref.[2]. Required amounts of $La_2O_3$ (99.99%), $SrCO_3$ (99.9%), $Ga_2O_3$ (99.99%) and MgO (99.99%) were mixed with the aid of acetone for one hour and fired at 1250 °C overnight. After regrinding and pelletizing, the pellitized mixture was finally sintered at 1470 °C for 36 hrs. All materials were examined by powder x-ray diffraction (Philips PW 1729) after their final calcinations.

SEM Observation

The microstructure of well-sintered and polished LSGM and LSGM-B were observed under a SEM (JEOL, JSM 35C). An appropriate thermal etching was used to reveal the grain boundaries and any second phase in the LSGM and LSGM-B samples.

Impedance Spectroscopy Measurement

Pt coatings obtained by pyrolysis were used as the electrodes in our two-probe ac-impedance spectroscopy measurements. Pt paste (from Heraeus) was applied to both ends of the LSGM or LSGM-B pellets, which were then baked at 900 °C for a half-hour. All conductivity measurements were made on cooling from 800 °C down to 320 °C. The impedance spectra of LSGM and LSGM-B cells were measured with a HP 4192A LF impedance analyzer in a range of frequency from 5 Hz to 13 MHz with an ac amplitude of 40 mV. In order to determine the chemical stability of the LSGM samples, atmospheres of pure oxygen, air, argon, argon + 2% $H_2$, argon + 10% $H_2$ and $H_2$ + 3% $H_2O$ were used in this measurement. The bulk and overall conductivities of LSGM were extracted from the intersections with the real axis of related bulk and grain-boundary semicircles in the impedance spectra.

Single Fuel Cell Tests

A round pellet of LSGM-B sample two inches in diameter after final sintering at 1470 °C was used as an electrolyte, $La_{0.6}Sr_{0.4}CoO_{3-\delta}$ (LSCo) was used as a cathode, and $CeO_2$+NiO or LSGM+NiO was used as an anode. The 500 μm thickness of the electrolyte membrane was obtained by grinding the sintered LSGM-B pellets on a diamond wheel.

In order to monitor the overpotentials on both the cathode and the anode reference, electrodes were constructed with the same materials as those corresponding to the working electrodes. The electrodes were fabricated on both surfaces of the thick-membrane electrolyte by screen-printing a slurry of an intimate mixture of electrode powder and organic binder (from Heraeus). After baking at 1125 °C for 2 hrs, Pt meshes with Pt leads were fixed on the top of each electrode to act as current collectors; corresponding electrode paste was added to achieve good electrical contacts. The effective electrode area of each cell to be tested in this study was 2.5 $cm^2$, and the thickness of the LSGM-B electrolytes was about 500 μm. These cells were finally glass-sealed onto $ZrO_2$ tubes at 1100 °C for 30 minutes because $ZrO_2$ has a similar thermal expansion coefficient to that of LSGM-based materials. The glass sealant used in this study was developed by Ceramatec, Inc.

The testing cells were placed into the hot zone of a vertical furnace. Air was supplied directly to the cathode surface. Water-moistened (at ~ 30 °C) hydrogen was flowing to the anode surface at a rate of 100 ml/min. All the tests and the heating/cooling of the furnace were controlled by a computer and performed from 600 to 800 °C. Tests were conducted potentiostatically from open-circuit voltage (OCV) to 0.4 V and back to OCV in steps of 20 mV and holding 10 seconds at each point.

## RESULTS AND DISCUSSION

X-Ray Diffraction

Fig. 1(a) shows an x-ray diffraction pattern of the LSGM sample. A second phase can be detected in the pattern; it is identified as $LaSrGaO_4$ (JCPDS 24-1208). The pattern of the improved sample LSGM-B is shown in Fig. 1 (b). Only a trace of the $LaSrGaO_4$ peaks was found.

SEM Observation

The microstructure under SEM of the polished LSGM after thermal etching at 1300 °C for 1 hr is shown in Fig. 2(a). The second phase, $LaSrGaO_4$, that was identified by XRD appears along the grain boundaries and within the grains. In contrast, the SEM microstructure of LSGM-B, Fig. 2(b), presents clear grain boundaries and grains. These observations agree well with the results of x-ray diffraction.

Impedance Spectroscopy

Fig. 3(a) shows the impedance spectrum of LSGM at 396 °C measured in air with Pt electrodes. It can be resolved into a grain semicircle, a grain-boundary depressed semicircle,

which is attributed to the second-phase $LaSrGaO_4$, and an electrode process arc. The grain-boundary effect involves a Constant Phase Element (CPE), and the depressed factor $\alpha = 0.05$ indicates that the second phase, $LaSrGaO_4$, is insulating to oxide-ion conduction (5).

The impedance spectrum of LSGM-B shown in Fig. 3(b) was measured under the same conditions as the LSGM sample; it can only be resolved into a grain semicircle and an electrode-process arc. The grain-boundary semicircle disappears with the absence of the second phase, $LaSrGaO_4$, as observed by XRD and SEM.

The overall oxide-ion conductivity at 800 °C, obtained from the intersection of the grain-boundary semicircle (or grain semicircle if no grain boundary exists) with the real axis, was raised from 0.094 S/cm for LSGM to 0.129 S/cm for LSGM-B. The reason for this conductivity enhancement is the elimination of the second phase and an increase of the oxygen vacancy concentration.

The dependence of overall conductivity $\sigma_o$ on the oxygen partial pressures $Po_2$ at different temperatures is displayed in Fig. 4. The near independence of $\sigma_o$ on $Po_2$ indicates a pure oxide-ion conduction and high chemical stability.

The long-term stability of the conductivity for sample LSGM is shown in Fig. 5. No degradation of conductivity at 600 °C was observed during one-week of measurement, indicating no oxygen vacancy ordering occurred.

Fig. 6 compares LSGM-based materials with other well-known oxide-ion conductors. It is apparent that doped $LaGaO_3$ is the best oxide-ion conductor having no reduction problem on exposure to the fuel reductant. Our new results present a $\sigma_o = 0.15$ S/cm at 800 °C and 0.07 S/cm at 700 °C, which is almost one order of magnitude higher than that of $ZrO_2$ at the same temperatures. Some conductivity data obtained in our lab were listed in Table I.

Table I. Typical conductivity data of some doped $LaGaO_3$ obtained in our lab

| T, °C<br>σ(total)<br>Samples | 800 | 702 | 595 |
|---|---|---|---|
| LSGM | 0.094 | 0.044 | 0.017 |
| LSGM-A | 0.105 | 0.053 | 0.018 |
| LSGM-B | 0.129 | 0.059 | 0.017 |
| LSGM-C | 0.150 | 0.068 | 0.021 |
| LSGM-D | 0.151 | 0.071 | 0.021 |
| LSGM-E | 0.146 | 0.074 | 0.025 |

Single Fuel Cell Tests

Based on the above results, LSGM-based materials are very strong candidates for the replacement of $ZrO_2$ in a SOFC. Fig. 7 presents the result of a single fuel cell test. With $La_{0.6}Sr_{0.4}CoO_{3-\delta}$ (LSCo) as the air electrode, LSGM-B as the electrolyte and $CeO_2$+NiO as the hydrogen electrode ($H_2$+3%$H_2O$), the usual open-circuit voltage of the cell is about 1.08 V and the maximum power density at 800 °C reaches 270 mW/cm$^2$ for a 500 μm thickness of the electrolyte. This result indicates an excellent performance of the fuel cells. Moreover, we found a high overpotential existing at the anode side, *e. g.* 500 mV at 700 mA/cm$^2$ current density, indicating that the anode has not yet been optimized. The trials with LSGM+NiO as anode give an even higher power-density output, but these anodes degraded with time quickly. Improved electrodes promise to give excellent performance for a thick-membrane SOFC operating in the range of 700 to 800 °C.

## CONCLUSIONS

A second phase, $LaSrGaO_4$, has been found in the previously identified superior oxide-ion conductor $La_{0.9}Sr_{0.1}Ga_{0.8}Mg_{0.2}O_{2.85}$ (LSGM); this phase is not an oxide-ion conductor and contributes to the grain boundary resistance. Nonstoichiometric doping of this material is found to eliminate the second phase and enhance the conductivity. Conductivity

measurements in different atmospheres ($Po_2$ = 1 - $10^{-22}$ atm) indicate a near independence on oxygen partial pressure and a high chemical stability. The conductivity was also stable over a long-term measurement at 600 °C. A single fuel cell test displayed a promising result. At 800 °C, the open-circuit voltage was about 1.08 V, close to the theoretical value, and the maximum power density was 270 mW/cm$^2$ for a 500-μm thick electrolyte with LSCo as cathode and $CeO_2$+NiO anode exhibiting high anode overpotential of 500 mV at 700 mA/cm$^2$. An LSGM+NiO anode yielded an even higher maximum power density, 320 mW/cm$^2$, under the same conditions, but it degraded rapidly with time.

## ACKNOWLEDGMENT

We would like to thank EPRI (Electric Power Research Institute) for the financial support and Ceramatec, Inc. for the single fuel cell tests. Dr. Wate T. Bakker is the EPRI manager of this project.

## REFERENCES

1. T. Ishihara, H. Matruda and Y. Takita, J. Am. Chem. Soc., **116**, 3801 (1994)
2. M. Feng and John B. Goodenough, Eur. J. Solid State Inorg. Chem., **T31**, 663-72 (1994)
3. K. Q. Huang, M. Feng and John B. Goodenough, J. Am. Ceram. Soc., **79** (4), 1100-104 (1996)
4. P. N. Huang and A. Petric, J. Electrochem. Soc. **143**, 1664 (1996)
5. K. Q. Huang, Man Feng and John B. Goodenough, submitted to J. Am. Ceram. Soc.
6. R. T. Dirstine, R. N. Blumenthal and T. F. Kuech, J. Electrochem. Soc., **126**(2), 264-9 (1979)
7. D. W. Strickler and W. G. Carlson, J. Am. Ceram. Soc., **47**(3), 122-7 (1964)
8. T. Takahashi, H. Iwahara, T. Arao, J. Appl. Electrochem., **5**, 187-95 (1975)